High-Resolution Investigation of Nanoparticle Interaction with a Model Pulmonary Surfactant Monolayer

Amit Kumar Sachan,[†,‡] Rakesh Kumar Harishchandra,[†] Christoph Bantz,[§] Michael Maskos,[§,⊥] Rudolf Reichelt,[‡] and Hans-Joachim Galla[†,*]

[†]Institute of Biochemistry, Westfälische Wilhelms Universität, Wilhelm-Klemm-Str.2, 48149 Münster, Germany, [‡]Institute of Medical Physics and Biophysics, Westfälische Wilhelms Universität, Robert-Koch-Str. 31, 48149 Münster, Germany, [§]Institute of Physical Chemistry, Johannes Gutenberg University, Jakob-Welder Weg 11, 55128 Mainz, Germany, and [⊥]Institut für Mikrotechnik Mainz (IMM), Carl-Zeiss-Str. 18-20, 55129, Mainz, Germany

ABSTRACT The pulmonary surfactant film spanning the inner alveolar surface prevents alveolar collapse during the end-exhalation and reduces the work of breathing. Nanoparticles (NPs) present in the atmosphere or nanocarriers targeted through the pulmonary route for medical purposes challenge this biological barrier. During interaction with or passage of NPs through the alveolar surfactant, the biophysical functioning of the film may be altered. However, experimental evidence showing detailed biophysical interaction of NPs with the pulmonary surfactant film are scant. In this study, we have investigated the impact of a hydrophobic polyorganosiloxane (AmOrSil20) NPs on the integrity as well as on the structural organization of the model pulmonary surfactant film. Primarily, scanning force microscopic techniques and electron microscopy have been used to visualize the topology as well as to characterize the localization of nanoparticles within the compressed pulmonary surfactant film. We could show that the NPs partition in the fluid phase of the compressed film at lower surface pressure, and at higher surface pressure, such NPs interact extensively with the surface-associated structures. Major amounts of NPs are retained at the interface and are released slowly into the aqueous subphase during repeated compression/expansion cycles. Further, the process of vesicle insertion into the interfacial film was observed to slow down with increasing NP concentrations. The hydrophobic AmOrSil20 NPs up to a given concentration do not substantially affect the structural organization and functioning of pulmonary surfactant film; however, such NPs do show drastic impacts at higher concentrations.

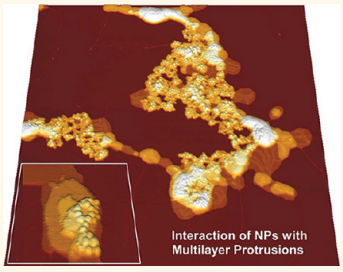

KEYWORDS: pulmonary surfactant · nanoparticle · surface-associated structure · protrusion · electron microscopy · phase imaging · vesicle insertion

The foremost requirement for normal breathing is a well functional, healthy, and stable pulmonary surfactant film, which spans the alveoli at the air–water interface. During inhalation and exhalation cycles of breathing, this film expands and compresses, respectively. Two apparently opposite but essential attributes of this interfacial film make it a unique protective lining. First, it withstands and forms a stable film at high surface pressure values up to 70 mN/m during end-exhalation to avoid fatal alveolar collapse, and second, it respreads rapidly and effectively during the next cycle of inhalation.[1,2]

The pulmonary surfactant layer in vertebrate lungs is a complex mixture of lipids and proteins. The content of lipids includes 85–90% (w/w), mainly phospholipids along with small amounts of cholesterol. Among phospholipids, the most abundant group is a zwitterionic phosphatidylcholine (PC) along with a second major compound, the negatively charged phosphatidylglycerols (PGs).[3] Individual component analysis of the pulmonary surfactant reveals that the disaturated dipalmitoylphosphatidylcholine (DPPC) lipid, which holds 40–50% (w/w) of the total pulmonary surfactant lipids, can sustain high surface pressures for long periods, but it shows poor respreading behavior at the onset of alveolar expansion.[4] The latter surface activity of the film, that is, respreading and adsorption, is exceeded through anionic PGs and unsaturated phospholipids, also called "good fluidizers", with the help of two hydrophobic surfactant proteins B (SP-B) and C (SP-C).[5,6] Each lipid–protein component within the surfactant film interacts with and complements each other during compression and expansion cycles. In addition, two hydrophilic proteins SP-A and SP-D are believed to play an important role in the storage and transport of lung surfactant materials as well as in the host defense.[7]

During compression of a pulmonary surfactant monolayer at high surface pressures, SP-B and SP-C proteins induce a reversible formation of multilayered protrusion structures ("surface-associated reservoirs") associated with the surface. The amount of

* Address correspondence to gallah@uni-muenster.de.

Received for review November 30, 2011 and accepted January 30, 2012.

Published online January 30, 2012
10.1021/nn204657n

protruded structures corresponds directly to the active surface area reduction within alveoli during exhalation. Structural evidence of the multilayered structures has been well confirmed, *in vivo* by means of electron microscopy[8] and *in vitro* by atomic force microscopy[9−11] as well as IR spectroscopy.[12] The formation of these multilayered structures is necessary to avoid alveolar buckle at high surface pressures. The interfacial layer at this stage, highly enriched in DPPC lipid, helps to withstand high surface pressures.[13] However, surface-associated protrusions, containing preferentially fluidizing lipids (PGs and unsaturated lipids) and surfactant proteins, readily restore into the surface layer during the next expansion cycle.[14]

Besides reducing the energy barrier for the breathing process, the pulmonary surfactant film also acts as a first line of barrier for any xenobiotics inhaled through the airways, which tend to enter the underlying cells. Because of continuous contact with the atmosphere, surfactant lining is destined to interact with micro/nanoparticles (NPs) as pollutants, produced by various natural as well as human processes such as smoking or combustion. NPs generated as a result of combustion processes such as automobiles, industrial chimneys, and fires are favorably carbonaceous and hydrophobic in nature and show predominant presence in the urban air pollution. NPs can have varying deleterious effects based on their shape, size, surface area to volume ratio, surface charge, surface coatings, electrical potential, and solubility.[15] Schleh *et al.*[16] have shown that nanosized but not microsized TiO_2 particles induce significant dysfunction of the pulmonary surfactant. Increasing use of NPs, especially metal NPs, in medical, industrial, and other purposes has led to the escalating chances of being exposed to such NPs through the air route *via* the pulmonary system. Previous studies taking account of metal NPs on pulmonary surfactant systems have shown moderate to drastic effects at different doses.[16,17] In addition, medically relevant nanocarriers, nanoprobes, and NPs targeted through the pulmonary route also challenge the surfactant layer.[18] However, since up to now the major focus has been to study the potential and systemic toxicology of such nanoentities inside the body, their biophysical impacts on the pulmonary surfactant film are least explored. Therefore, having the physiological importance of this surface monolayer in mind, it is indispensable to investigate any destabilizing effects of NPs on this lipid−peptide film.

Owing to the complex nature of the natural pulmonary surfactant, a well-defined and highly reproducible molecular pulmonary surfactant model has been developed and successfully used, which contains zwitterionic DPPC and negatively charged DPPG along with surfactant-specific protein C.[19−21] Previously, we have shown using epifluorescence microscopic technique that polyorganosiloxane NPs interact with the lipid monolayer and considerably disturb the domain structures by a reduction of the line tension.[22] In this study, we have investigated the biophysical interaction of the hydrophobic polyorganosiloxane NPs (AmOrSil20: 19 ± 3.2 nm in diameter) as a model for air pollutants and medically relevant carriers, with the artificial pulmonary surfactant film using Langmuir film balance, atomic force microscopy (AFM), and dark-field electron microscopy techniques. Langmuir film balance experiments have been conducted to characterize the surface activity and integrity of the model surfactant film in the presence of NPs. The potential of an AFM has been utilized extensively to characterize (1) the presence of NPs within the compressed film, (2) retention of NPs at the interface, (3) interaction of NPs with the surface-associated structures, (4) the influence of NPs on the area as well as volume of the protrusion structures, and (5) opsonization of NPs by the surfactant components. In addition, the effect of NPs on the vesicle insertion process at the monolayer surface has been analyzed.

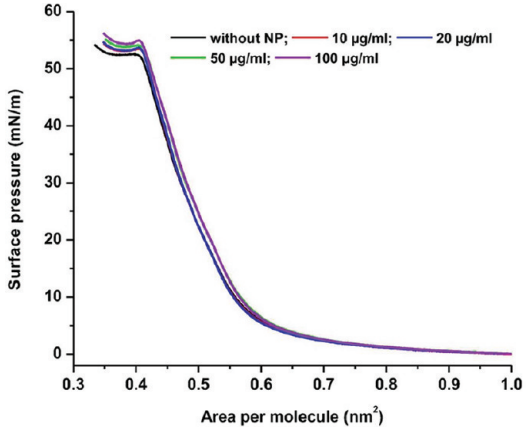

Figure 1. Surface pressure−molecular area (π−A) isotherms of DPPC/DPPG/SP-C (80:20:0.4 mol %) film incubated without and with different concentrations of AmOrSil20 NPs (10, 20, 50, 100 μg/mL).

RESULTS AND DISCUSSION

Surface Activity of Pulmonary Surfactant in the Presence of NPs. The compression isotherm of the model pulmonary surfactant layer has a typical shape as reported earlier.[20] During compression of the surfactant monolayer containing SP-C, the surface pressure increases up to a value of around 53 mN/m and remains constant upon further compression, forming a pronounced plateau region. The presence of this plateau region is explained by the formation of three-dimensional bilayer stacks, representing the protrusions, associated with the surface layer. These protrusions allow the compression of the monolayer without further increase in the surface pressure. The isotherms of model pulmonary surfactant films without nanoparticles as well as with different concentrations of NPs (10, 20, 50, and 100 μg/mL) are shown in Figure 1. In the presence of NPs, isotherms show a minor molecular area shift

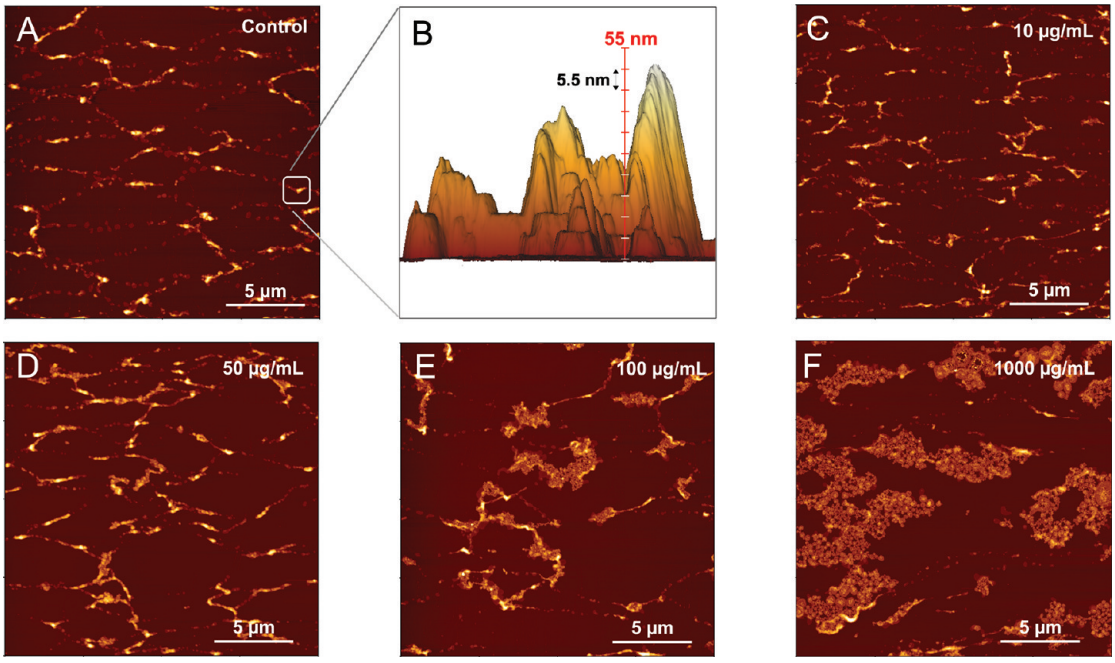

Figure 2. AFM intermittent contact mode topography images. (A) Compressed model pulmonary surfactant (DPPC/DPPG/SP-C) film (control). (B) Three-dimensional view of a multilayer protrusion region showing bilayer steps (marked by each tick on *z*-scale). (C–F) Pulmonary surfactant film incubated and compressed with different concentrations of AmOrSil20 NPs. All of the films were transferred at ~52.5 mN/m surface pressure. The *z*-range is 0–80 nm for images A,C–F.

toward higher areas. The plateau pressures of the surfactant films co-spread with varying concentrations of NPs move toward higher surface pressure values, whereas the shape of the plateau remains unchanged. Thus, the presence of NPs up to 100 μg/mL concentration within pulmonary surfactant does not show a major influence on the surface activity as well as on the integrity of the monolayer during compression.

Partitioning of NPs within Compressed Pulmonary Surfactant Film. The pulmonary surfactant monolayer film forms surface-associated multilayer protrusions upon compression at the plateau pressure. These multilayer protrusion structures have been visualized after transfer of such a film on a solid support through AFM topographical study.[11,20] Figure 2 shows intermittent contact (IC) mode imaged topographical features of the model pulmonary surfactant film compressed to a surface pressure of ~52.5 mN/m in the absence and presence of NPs. Each topograph can be divided in two major sets of structures: first, networks of bright regions, and second, dark brown polygonal shaped regions. Bright regions in networks consist of multilayer structures, ranging in height from single bilayer (~5.5 nm) to collapsed heightened protrusions (up to 75–85 nm). Protrusions demonstrate distinct bilayer, tetralayer, hexalayer, octalayer, decalayer, and even higher collapsed structures of pulmonary surfactant components, such as lipids and SP-C protein. A three-dimensional view of a protrusion region is shown in Figure 2B.

Like pure pulmonary surfactant (Figure 2A), all of the NP-containing samples show almost similar range of heights of protrusion structures even at high concentrations of NPs (1000 μg/mL) (Figure 2C–F). In the presence of NPs, the polygonal shaped domains show a clear increase in size while shape is affected too, which is well evident at high concentrations. Moreover, distinct nanoscale globular structures in clusters, associated with protrusions, appear in all of the NP-containing samples. The quantity of such clusters increases with increasing concentrations of NPs in the surfactant, and at very high concentrations of NPs such as 1000 μg/mL, these nanoscale globular structures predominate over protrusions (Figure 2F). The clusters primarily show two-dimensional aggregation, and the height range of a majority of these clusters lies between 15 and 35 nm. These clusters may belong to NP clusters themselves or globular lipid structures induced by NP presence or both. Occasionally, similar globular structures are also seen in control samples (data not shown). However, lateral diameter of nanoscale globular structures shows higher values than the respective height, and if these globular structures belong to NPs, increase in their lateral diameter can be due to dilation effect of tip shape/radius.

In order to characterize the presence of NPs within the compressed film, force modulation microscopy (FMM) technique was employed. In a typical FMM experiment, the tip is oscillated vertically in a repulsive regime at a certain frequency, well below its resonance frequency, with an amplitude of a few nanometers, and the changes occurring in the amplitude signal while scanning are correlated to the spatial variations in the mechanical properties on the sample surface such as elasticity, viscoelasticity, or adhesion.[23–25]

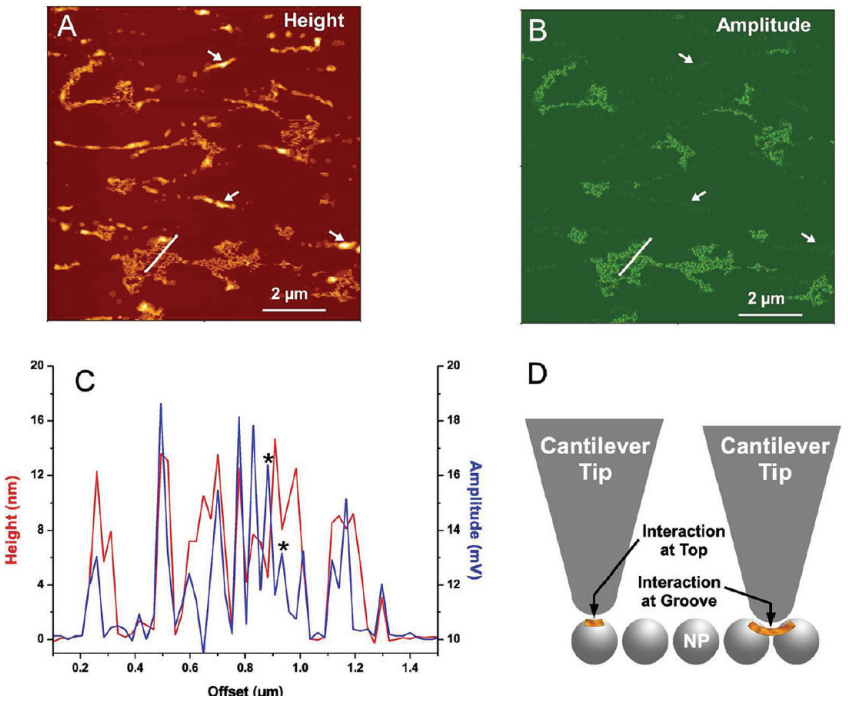

Figure 3. Force modulation microscopy of compressed (52.5 mN/m) pulmonary surfactant film containing 100 μg/mL NPs. (A) Topography and (B) amplitude signal. Bright colors within the image represent high values of the signals. Marked arrows indicate high protrusion structures in panel A and their respective amplitude signals in panel B. (C) Overlapped height and amplitude cross-section profiles, where asterisks indicate high amplitude signals arising from the crevices present between two successive height signal peaks. (D) Schematic of the interaction of the cantilever tip at the top of NPs and at the grooves present between NPs.

We performed the FMM experiments with less invasive parameters on the NP-containing films to qualitatively compare the stiffness differences across the sample, as NPs are believed to be harder spheres[26] than lipid layer structures. Figure 3A,B shows the topography and amplitude signals, respectively, of an FMM experiment on a film containing NPs (100 μg/mL). The color scale pattern of the FMM topograph and amplitude signal image is similar to the IC mode topographs. Like IC mode topography, FMM topography shows a similar pattern of structures in the NP-containing films, with minor dragging effects due to the lateral forces associated with this mode of imaging. In the amplitude signal image, lipid layered structures including heightened protrusions (Figure 3B, marked by arrows) do not yield significant amplitude contrast as these structures are expected to exhibit similar elasticity behavior. However, a few structural features across the scanned surface provide higher amplitude signals than the rest of the area. The areas of higher amplitude signals are believed to reflect the places of higher elastic modulus or stiffness. Superimposition of amplitude signal image on the topography image reveals that the higher amplitude signals overlap well on the places of nanoscale globular clusters in the topograph. Hence, it indicates that the higher amplitude signals originate from the nanoscale globular clusters.

To compare as well as to determine the source of amplitude signals at the nanoscale, height and amplitude signal profiles across the same cross section of the nanoscale globular cluster were extracted and superimposed (Figure 3C). Overlapping amplitude signal peaks with the peaks of height signal (top of globular structures) indicate the origin of such higher amplitude signals from a relatively stiffer sample surface, which can be none other than the NP's top surface, as lipid structures did not yield significant amplitude signals. Thereby, nanoscale globular structures are substantiated to be NP clusters. However, a few higher amplitude signals arise from the crevices present between two successive height signal peaks (Figure 3C, marked by asterisk). These signals can arise due to an increased contact area between tip and sample[27] at such places ascribed to grooves (Figure 3D).

Furthermore, to analyze any changes in the NPs' morphology due to surfactant components, electron microscopy dark-field imaging of the pulmonary surfactant film containing NPs was performed. The compressed film transferred from the Ca^{2+} buffered subphase was unable to provide sufficient image contrast for the lipid layer structural steps, which may be due to strong electron scattering by Ca^{2+} ions,[28] associated with the lipid head groups (data not shown).[29] However, the high-resolution dark-field electron microscopy image of the film transferred from the aqueous subphase yields good contrast, and lipid bilayer and tetralayer structures can be easily identified based

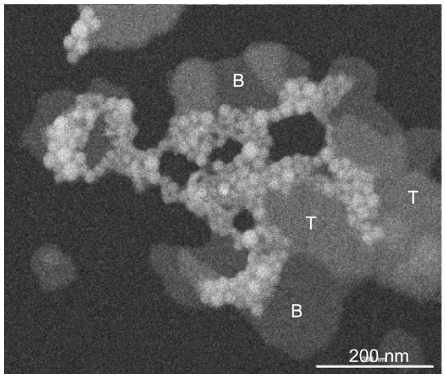

Figure 4. Dark-field electron microscopy image of (unstained) pulmonary surfactant film containing 50 μg/mL NPs transferred at 52.5 mN/m from pure water subphase. In the image, B and T represent bilayer and tetralayer protrusion structures, respectively.

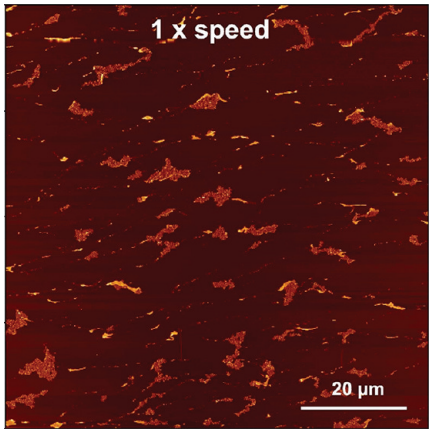

Figure 5. AFM intermittent contact mode topography image of a surfactant film containing 100 μg/mL NPs transferred at 52.5 mN/m after nine compression cycles. The *z*-range is 0−90 nm.

on the contrast of the respective structure. Besides, two-dimensional NP clusters closely associated with the multilayer structures are seen without any significant change in particles' morphology (Figure 4). Also, diameters of the NPs appear to be around 20 nm as expected. To the best of our knowledge, it is the first study to present *in vitro* multilayer protrusion structures within a compressed pulmonary surfactant film transferred on an EM grid, without any staining or coating of the sample.

In the absence of an analytical energy-filtered electron microscope, materials (consist of lightweight elements) harboring low electron scattering character are hard to distinguish and characterize from the background lipid structures. Hence, the qualitative study by the FMM and the size and shape results from the dark-field electron microscopy imaging manifest well the presence as well as retention of NPs within the compressed pulmonary surfactant film. In addition, AFM topography studies of the NP-containing films compressed up to plateau surface pressure show vivid association of "NP clusters" with the multilayer protrusion structures, which derive from the fluid phase (at lower surface pressure) components of the surfactant film.[30] Here it is worthy to mention that such NPs at lower surface pressure show selective partitioning within the fluid phase of the pulmonary surfactant monolayer (Supporting Information Figure S1).

Retention of NPs at the Interface. We examined the retention of AmOrSil20 NPs within the surfactant films at the interface with respect to additional factors: prolonged incubation time (1−4 h) at the interface, increased compression−expansion cycles, and different speeds of the compression−expansion process. The AFM topography analysis was performed to observe the presence as well as to visually estimate the retention of NPs in the compressed film. Multiple images of larger scan area (80 × 80 μm^2) were examined. Figure 5 shows a topograph of NP-containing film transferred after nine compression cycles (1*x* speed, where *x* is the initial speed of compression). Additional cycles of compression and expansion lead to minimal amount of NP translocation in the subphase while retaining the maximal amounts as compared to the film transferred after the first compression cycle (1*x* speed).

Despite unmatched barrier speed of Langmuir film balance with the physiological breathing rate, we performed the hysteresis experiments at different barrier speeds (1.5*x*, 2*x*, and 4*x*) to scrutinize any significant effect caused by the speed on the retention property of the NPs. AFM topographs show again that the majority of the NPs are still not able to translocate across the surface and are retained in the film (Supporting Information Figure S2). Although this analysis at varying speeds cannot be compared with the physiological rates, it surely indicates that such hydrophobic NPs are experiencing a high free energy barrier at the interface even at the lowest surfactant density occurring during complete expansion phases of hysteresis cycles. However, pure AmOrSil20 NPs without lipids are unable to sustain high surface pressures (above 21 mN/m) at the interface and collapse in the subphase on further compression or expansion.[22] The development of such a high free energy barrier for these NPs in the presence of pulmonary surfactant can be explained *via* a strong interaction between hydrophobic NPs and the components of pulmonary surfactant at the interface. Our finding shows good concordance with the molecular dynamics simulation works performed on the hydrophobic NPs at the pulmonary surfactant monolayer, which suggest that the presence of a high free energy barrier for such NPs prevents them from translocating into the subphase spontaneously.[31,32] In contrast, hydrophilic hydroxyapatite NPs have been shown to readily penetrate the pulmonary surfactant layer after exposure.[33]

Interaction of NPs within the Surface-Associated Structures. To provide clear illustration of interaction of NPs within

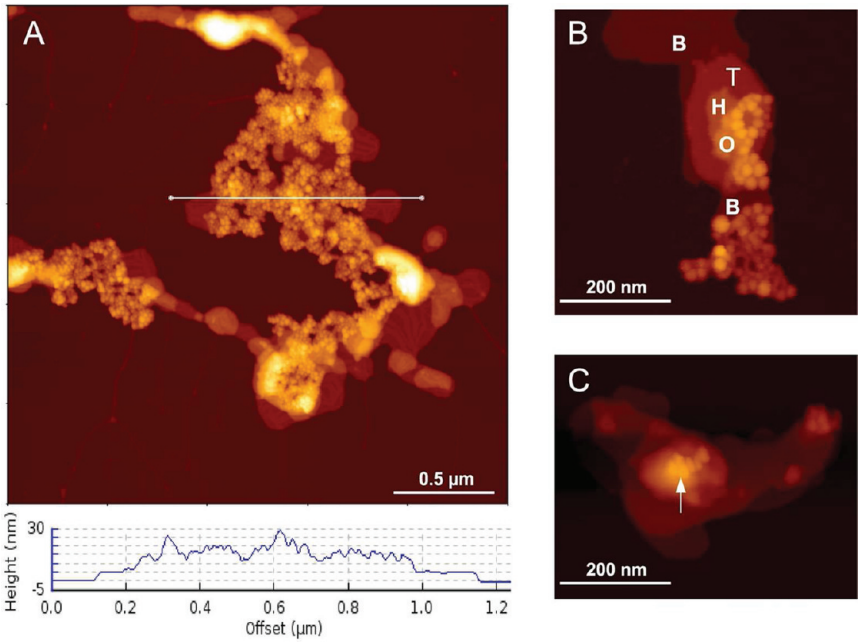

Figure 6. High-resolution intermittent contact mode topography images of pulmonary surfactant films containing 50 μg/mL NPs transferred at 52.5 mN/m (A−C). Image A shows intense interactions of NPs with the protrusion structures and height profile of a cross section. Image B shows evident close interactions of NPs with the surfactant bilayer, tetralayer, hexalayer, and octalayer structures. Image C depicts the presence of NPs on top of a high protrusion structure (marked by an arrow).

the interfacial pulmonary surfactant film at plateau surface pressure, we performed high-resolution imaging in the IC mode at comparatively small area ($\leq$2.5 μm $\times$ 2.5 μm). The feedback settings for the imaging were optimized to yield better topography profile, and sharp tips were used to minimize dilation effect due to tip shape/radius. High-resolution topography study shows that the NPs, within the compressed film, do not appear to preferentially localize at the boundaries of polygonal shaped domains, which correspond to liquid condensed phase at lower surface pressure. However, NPs appear to be closely associated with the surface-associated structures (Figure 6A). Figure 6B illustrates direct association of NPs with the bilayer, tetralayer, hexalayer, and octalayer protrusion structures, and such interactions were found irrespective of NP concentrations within the surfactant film. Besides these interactions with protrusion structures, NPs also reside as small ($\sim$100 nm) to big (2−8 μm) individual clusters depending on the NP concentration. On the basis of the lateral forces required to dislodge the NPs, NPs interacting with the protrusion structures show more firm association than the NPs present as an isolated cluster (data not shown). As shown in Figure 6C, NPs are also found on top of the collapsed heightened protrusion structures ($\sim$55 nm). Possible confinement of NPs within the heightened protrusions cannot be ruled out, but we are hitherto unable to observe them. We believe that such direct interaction of NPs with the lipid layer structures can possibly interfere with the surfactant respreading phenomenon at the onset of next expansion cycle.

Effect on the Area and Volume of the Surface-Associated Protrusion Structures. A close scrutiny of the topographs of control and NP-containing samples reveals that the frequency as well as area occupied by the high protrusion structures (>35 nm in height) decreases as the NP concentration in the sample increases. To analyze the effect of NPs on the lateral distribution as well as on the amount of protruding structures, statistical analysis of the area and volume occupied by the high protrusions in the control and NP-containing samples was performed. The pixel values $\geq$35 nm in height were selected to minimize possible error due to NP clusters' height (15−35 nm) in the analysis of protrusion structures. Area analysis shows a clear decrease of area occupied by the protrusion structures with increasing concentrations of NPs (Figure 7A). Similar trends of results were obtained from the volume analysis of such structures (Figure 7B). Both area and volume decreases by 50−60% at high concentration of NPs with respect to the control. Such influence on the frequency, area, and volume of protrusions may be explained by plausible sequestration of protrusion structures' components, mainly DPPG and SP-C, around NPs. Such depletion can hinder the formation or reduce the extent of surface-associated structures. Although SP-C is present in a very small quantity in the surfactant, it plays a pivotal role in the transition of two-dimensional monolayer into the three-dimensional multilayer protrusions. Sequestration of even a small amount of hydrophobic SP-C around hydrophobic NPs can have drastic effects on the multilayer protrusions.

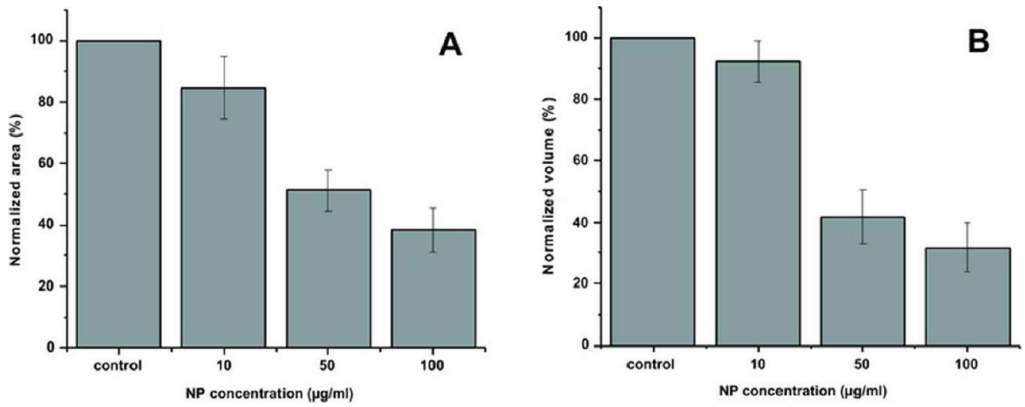

Figure 7. Analysis of the lateral area (A) and the volume (B) occupied by the high protrusion structures (≥35 nm) present within the control and NP-containing pulmonary surfactant films. All NP-containing sample data are normalized with the control and expressed as mean ± SD (n = 20).

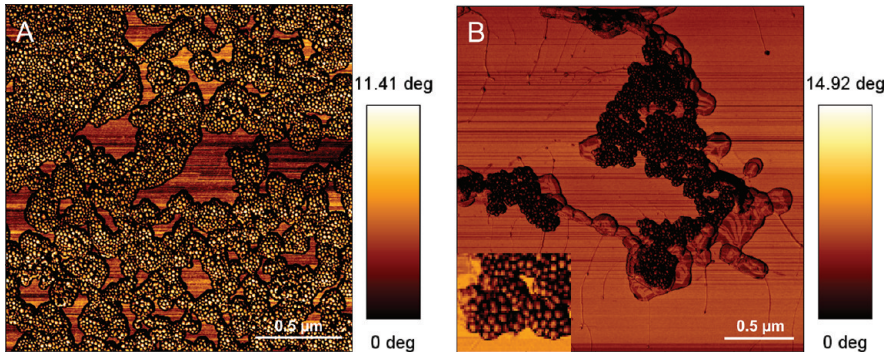

Figure 8. High-resolution phase images recorded at A_{sp}/A_o ratio of 0.6. Phase image of (A) bare hydrophobic NPs transferred on mica and (B) pulmonary surfactant film containing 50 μg/mL NPs. Inset shows a magnified view of phase shift contrast on the top of NPs present within the pulmonary surfactant film. The z-range is (A) 0−12° and (B) 0−15°.

Opsonization of NPs by the Surfactant Components. To further investigate the interaction of surfactant components with NPs and a possible opsonization of the NPs, phase imaging was performed. Phase imaging is a secondary mode derived from the IC mode. It generates a map of phase shifts occurring between the cantilever oscillation and the piezo-driven oscillation while scanning across the sample surface. Phase shift contrast reflects variation in the conservative and/or dissipative forces[34−36] between two points on the sample image, which can be carefully used to delineate the sample surface property variations such as chemical composition, adhesion, hydrophobicity−hydrophilicity, elasticity, or viscoelasticity.[23,35,37,38] It is worth mentioning that the origin of phase shift is a complex phenomenon, and more than one factor can have an influence on the phase shift signal.[39−41] Previously, it has been shown that a phase advance or positive phase shift is observed when a hydrophilic tip interacts with a hydrophobic surface, which is expected to be a rather repulsive interaction. Moreover, attractive interaction between a hydrophilic tip and a hydrophilic surface results in a phase lag or negative phase shift.[37,38]

We performed the phase imaging on the bare hydrophobic AmOrSil20 NPs transferred on mica as well as on the surfactant film containing NPs to unravel the surface property changes on the top of the NPs as a result of incubation and compression with the surfactant components. Figure 8A shows the phase image of bare NPs transferred from the aqueous subphase onto mica, where the top of the NPs shows a more positive phase shift of about 5° compared to the mica background. Mica is well-known to exhibit a hydrophilic surface, whereas bare AmOrSil20 NPs are distinctly hydrophobic. Therefore, differential interactions of the hydrophilic silicon tip with the hydrophilic mica and with the hydrophobic NPs are expected to be observed in the phase image.

In a similar approach, the interaction strength was analyzed on the surfactant film containing NPs. As expected, lipid multilayer structures, bilayers to heightened protrusions, show almost no phase shift contrast in the phase images of NP-containing samples (Supporting Information Figure S3A,B, pointed arrows). Figure 8B shows the high-resolution phase image of the NP-containing sample which provides better visible resolution at the places of NP clusters. Here, areas at the top of NP clusters clearly show more negative phase shift signals than associated multilayer structures (Figure 8B, inset). Hydrophobic nature, hard

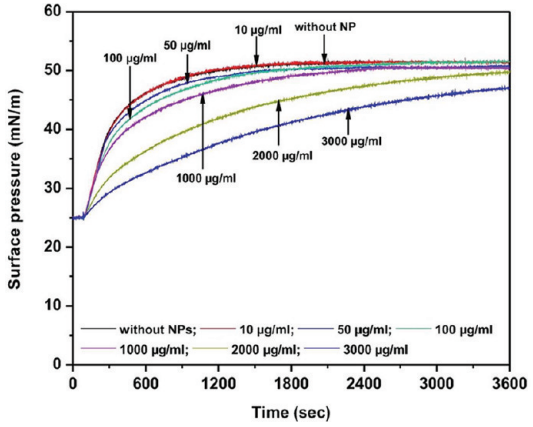

Figure 9. Vesicle insertion kinetic studies of DPPC/DPPG/SP-C (0.4 mol %) monolayer with different concentrations of NPs at surface pressure of 25 mN/m. All of the measurements are performed on subphase containing 25 mM HEPES and 3 mM $CaCl_2$, pH 7.0.

sphere, comparatively least possible water adsorption on the NP surface, and the least available contact area for the cantilever tip on top of NPs—all these properties are supposed to facilitate phase advance signals rather than phase lag signals from the top of NPs compared to surrounding lipid structures. Hence, we conclude from the acquired phase lag signals that an attractive interaction occurs between tip and the NP surface, which can result due to possible NP coverage with lipids, where fatty acid tails are oriented toward the NP surface whereas hydrophilic headgroups are exposed to the cantilever tip. We thus conclude that the NPs localized in the compressed pulmonary surfactant film are opsonized by the surfactant components.

Vesicle Insertion Kinetic Studies. The natural pulmonary surfactant film experiences a continuous exchange of surfactant material between interface and subphase for the replenishment and recycling of surfactants, which is vital for the integrity and functioning of this safety lining.[42] The model pulmonary surfactant monolayer has been used to mimic the process of replenishment of surfactants, which occurs in two steps: initial adsorption of vesicles on the monolayer and subsequent fusion and integration in presence of Ca^{2+}.[43,44] In the present study, we have used unilamellar lipid vesicles, DPPC/DPPG (80:20 molar ratio), to mimic the insertion of new surfactant materials into the model pulmonary surfactant monolayer.

Figure 9 shows the kinetics of vesicle insertion into the compressed monolayer containing different concentrations of AmOrSil20 NPs (10, 50, 100, 1000, 2000, and 3000 μg/mL) at surface pressure of 25 mN/m. In the presence of low NP concentration (10 μg/mL), the insertion rate is not influenced and is similar to the control. Increasing the NP concentration to 50 and 100 μg/mL slightly decreases the insertion rate, while further increasing the NP concentration up to 3000 μg/mL causes the insertion process to slow down drastically. It has been proposed that the fluid regions are crucial areas to which vesicles make contact followed by protein-facilitated insertion into the monolayer.[45] The surfactant-specific protein C prefers to be localized in the fluid phase of the monolayer,[14] and as reported here, this is also true for the NPs. Hence, we assume hthat the interaction of hydrophobic NPs with the surfactant proteins makes them unavailable for the insertion process and subsequently slows down the rate of vesicle insertion. Besides, increased spanning of fluid phase regions by the increasing NP concentrations may also compromise the available free fluid phase monolayer for the insertion process. Henceforth, we conclude that the NPs' presence in the monolayer is able to significantly inhibit the process of surfactant material insertion at least at high concentrations.

CONCLUSION

Hydrophobic nanoparticles are abundant in the atmosphere. We found that exposure of hydrophobic AmOrSil20 NPs to the model pulmonary surfactant does not significantly destabilize the film at the interface and, up to a certain concentration, will not compromise the structural organization and functioning of the pulmonary surfactant film except maybe under certain predisposed pulmonary diseases. However, drastic effects are seen at higher NP concentrations. While selectively partitioned at lower surface pressure in the fluid phase of the surfactant film, these NPs exhibit an intense association with the surface-associated protrusions at the plateau surface pressure. It is conceivable that the firm interaction of NPs with surface-associated structures can possibly affect the respreading phenomenon of such surfactant reservoir structures at high concentrations at the onset of the next expansion cycle. The finding is that the insertion kinetics of vesicles with the surfactant surface could be of importance since it shows for the first time that NPs interfere with the regeneration of the surfactant, which is an important process *in vivo*. From the fact that the NPs are unable to spontaneously translocate into the subphase from the interfacial pulmonary surfactant film and slowly release from the surface layer under repeated compression/expansion cycles, we conclude that the presence of surfactant monolayer at the interface offers a high free energy barrier for such hydrophobic NPs due to their interaction and association with the surfactant components and structures. Hence, according to our results, similar hydrophobic nanocarriers/particles targeted through the pulmonary route will tend to have much slower release than hydrophilic NPs[33] from the interface. This hindrance can, in fact, be utilized to specifically target such NPs as carriers to the surface layer in order to recycle the exhausted

surfactants. Moreover, these nanospheres, due to their core−shell structure, offer a great potential for a variety of biomedical applications through modification of their core.[46]

MATERIALS AND METHODS

Materials. The phospholipids 1,2-dipalmitoyl-*sn*-glycero-3-phosphocholine (DPPC) and 1,2-dipalmitoyl-*sn*-glycero-3-phosphoglycerol (DPPG) were purchased from Avanti Polar Lipids Inc. (Alabaster, AL) as a dry powder and used without further purification. SP-C protein was isolated from porcine bronchoalveolar lavage by the butanol extraction method.[47] HPLC grade chloroform and sodium salt of ethylenediaminetetraacetic acid (Na-EDTA) were purchased from Sigma-Aldrich (Steinheim, Germany), and HPLC grade methanol, *N*-2-(hydroxyethyl)piperazine-*N*′-2-ethanesulfonic acid (HEPES), and calcium chloride ($CaCl_2$) were purchased from Merck (Damstardt, Germany). Water was purified and deionized by a multicartridge system (Sartorius, Goettingen, Germany), yielding 0.055 μS/cm conductivity at 25 °C. Lipids were dissolved in chloroform/methanol solution (1:1, v/v).

Sample Preparation. Polyorganosiloxane nanoparticles (NPs), named "AmOrSil20", were synthesized in aqueous dispersion by co-condensation of a mixture of alkyldialkoxysilanes and alkyltrialkoxysilanes in the presence of surfactant. By sequential addition of mixtures with different ratios of bi- to trifunctional monomers, a core−shell architecture with different cross-linking densities can be realized. By final addition of tetramethyldisiloxane, a nonfunctionalized surface with hydrophobic properties is obtained. The particles have a hydrodynamic diameter of 24 nm, characterized by asymmetrical flow field−flow fractionation (in toluene) and a mean diameter (in dried state) of 19.4 ± 3.2 nm, determined from transmission electron microscopy images. Details of the synthesis and characteristics of this nanoparticle have been published elsewhere.[26,48] The particles were dissolved in chloroform to get a concentration of 10 mg/mL (1.93×10^{15} particles/mL). The sample solutions were prepared by mixing lipid solution (1 mg/mL) with varying concentrations of NPs: 10, 20, 50, 100, 1000, 2000, and 3000 μg/mL. The lipid−nanoparticle samples in chloroform/methanol solution were sonicated prior to spreading on the subphase.

Surface Pressure−Area Isotherms. All of the surface pressure/area isotherms were recorded on an analytical Wilhelmy film balance (Riegler and Kirstein, Mainz, Germany) with an operational area of 144 cm^2 at the subphase temperature of 20 °C. The subphase contained 25 mM HEPES and 3 mM $CaCl_2$ (pH 7.0). Desired samples were spread at the air/subphase interface. After an equilibration time of 10−15 min, allowing the solvent to evaporate, monolayer was compressed at a rate of 3 cm^2/min.

Langmuir−Blodgett (LB) Transfer. LB films were prepared by spreading the lipid−protein mixture with and without NPs on a film balance (Riegler & Kirstein, Mainz, Germany) with an operational area of 39 cm^2. All transfers were performed from buffer containing 25 mM HEPES and 3 mM $CaCl_2$ at 20 °C at constant molecular area and surface pressure. Prior to spreading, a freshly cleaved mica sheet (Electron Microscopy Science, Munich, Germany) was dipped vertically into the subphase. After an equilibration period, the monolayer was compressed with a velocity of 1.5 cm^2/min until the surface pressure of 52.5 mN/m was reached (just below the plateau region) to avoid a large shift in the molecular area prior to the film transfer. The monolayer was equilibrated at the specified surface pressure for another 10 min and then transferred onto mica with a velocity of 0.7 mm/min. For the NP retention experiment, the film was subjected to eight hysteresis cycles (surface pressure range: 0−52.5 mN/m), and at the end of the next compression cycle, the film was transferred onto mica as mentioned above.

Atomic Force Microscopy (AFM). AFM imaging of the compressed film transferred on mica sheet was performed using a NanoWizard II AFM (JPK Instruments, Berlin, Germany) operating in intermittent contact (IC) and force modulation modes in air at room temperature. Point Probe Plus (PPP)-NCHR (Nanosensors, Neuchatel, Switzerland) tips with resonance frequency of 270−300 kHz and spring constant of 42 N/m were used for IC mode imaging. To acquire height and phase images in IC mode, cantilevers were oscillated slightly below their resonance frequency, and the ratio of the amplitude of the set-point oscillation (A_{sp}) to the free oscillation (A_o) was set between 0.5 and 0.7. For force modulation microscopy (FMM), PPP-FM tips with spring constant of ∼2.8 N/m and resonance frequency of 60−70 kHz were used. The modulation amplitude and frequency were equal to 1−3 mV and 1 kHz, respectively. All images were obtained at 512 × 512 pixel resolution except where mentioned at the scan rate of 0.3−0.6 Hz. The image processing and cross-section profiling of height, amplitude, and phase images were performed using JPK image processing software.

Image Analysis. All AFM images (20 × 20 μm^2) were flattened before statistical analysis, and the pixels were subsequently extracted from images. Pixels above the offset value were selected and counted. For area analysis, count of selected pixels was multiplied by individual pixel area. For volume analysis, the height values of the selected pixels were redefined from the offset value, and then redefined height values were multiplied by individual pixel area to get the volume data. Origin (Northampton, MA) software was used for the data analysis.

Electron Microscopy. Usual LB transfer was performed to transfer a compressed surfactant film (∼52.5 mN/m surface pressure) on the holey carbon-coated copper grids, supported on a flat thin holder. Dark-field images (1000 × 800 pixels) of the unstained transferred film were recorded in digital form using the high-resolution field-emission scanning electron microscope (S-5000, Hitachi Ltd., Japan), in transmission mode, operated at 30 keV at room temperature. Images were acquired at an electron dose between 250 and 350 e^-/nm^2. The microscope was extended with a sensitive annular dark-field (ADF) detector to collect the signals in transmission mode.

Vesicle Preparation. DPPC/DPPG (80:20 molar ratio) was dissolved in chloroform/methanol (1:1, v/v) and dried under a stream of nitrogen at 50 °C. Traces of solvent were removed by keeping under vacuum at 50 °C overnight. The lipid films were hydrated by adding a preheated buffer containing 25 mM HEPES and 0.1 mM EDTA (pH 7.0). The vesicle suspension (5 mM) was kept for 30 min at 50 °C in a water bath and was vortexed for 30 s at regular intervals to get multilamellar vesicles (MLVs). The resulting MLVs were converted into large unilamellar vesicles (LUVs) at 50 °C by membrane extrusion using the LiposoFast (Avestine Europe GmbH, Mannheim, Germany) extruder containing a polycarbonate membrane with a pore diameter of 100 nm.

Vesicle Insertion Studies. The vesicle insertion experiments were performed using a lipid−peptide monolayer composed of DPPC/DPPG/SP-C (0.4 mol %). The monolayers containing different concentrations of NPs were formed at the air/water interface of a Wilhelmy film balance by spreading the respective samples from chloroform/methanol (1:1, v/v) onto the aqueous surface. The subphase consisted of 25 mM HEPES and 3 mM $CaCl_2$ (pH 7.0) and was stirred continuously by a magnetic bar. The monolayer was compressed with a computer-controlled barrier to a defined surface pressure and maintained for 10 min. The vesicle suspensions were then injected through an injection port into the subphase with a Hamilton syringe. The final lipid concentration in the subphase was 20 μmol/L. The lipid vesicle insertion was studied by monitoring the changes in surface pressure with respect to time at constant surface area at 20 °C. The studies were carried out over a period of 3600 s.

Conflict of Interest: The authors declare no competing financial interest.

Acknowledgment. The authors like to acknowledge the initial input of Prof. Dr. R. Reichelt, with whom we started this project but who unfortunately passed away too early and could not live to see the outcome. This project was supported by grant funds from DFG SP1313 programme and the BMBF "NanoGEM" consortium. We would like to thank for financial support NRW Graduate School of Chemistry to R.K.H. and Institute of Medical Physics and Biophysics (IMPB) to A.K.S. We thank S. Wulff, IBC, and A. Ricker, IMPB, for technical assistance, and U. Keller, IMPB, for the dark-field electron microscopy imaging. We are also thankful for the DFG grants RE 782/11-1 and RE 782/11-2 (for dark-field electron microscopy) to R.R.

Supporting Information Available: Supplementary experimental results. This material is available free of charge *via* the Internet at http://pubs.acs.org.

REFERENCES AND NOTES

1. Goerke, J. Lung Surfactant. *Biochim. Biophys. Acta* **1974**, *344*, 241–261.
2. Hills, B. A. The Role of Lung Surfactant. *Br. J. Anaesth.* **1990**, *65*, 13–29.
3. Veldhuizen, R.; Nag, K.; Orgeig, S.; Possmayer, F. The Role of Lipids in Pulmonary Surfactant. *Biochim. Biophys. Acta* **1998**, *1408*, 90–108.
4. Veldhuizen, E. J.; Haagsman, H. P. Role of Pulmonary Surfactant Components in Surface Film Formation and Dynamics. *Biochim. Biophys. Acta* **2000**, *1467*, 255–270.
5. Goerke, J. Pulmonary Surfactant: Functions and Molecular Composition. *Biochim. Biophys. Acta* **1998**, *1408*, 79–89.
6. Weaver, T. E.; Conkright, J. J. Function of Surfactant Proteins B and C. *Annu. Rev. Physiol.* **2001**, *63*, 555–578.
7. Reid, K. B. Functional Roles of the Lung Surfactant Proteins SP-A and SP-D in Innate Immunity. *Immunobiology* **1998**, *199*, 200–207.
8. Schurch, S.; Qanbar, R.; Bachofen, H.; Possmayer, F. The Surface-Associated Surfactant Reservoir in the Alveolar Lining. *Biol. Neonate* **1995**, *67*, 61–76.
9. Galla, H.-J.; Malcharek, S.; Bourdos, N. Analysis of Surface Topology and Chemical Composition of Microstructures Formed in Planar Surfactant Films under Compression. *ChemInform* **2006**, *37*, 247–270.
10. Krol, S.; Ross, M.; Sieber, M.; Kunneke, S.; Galla, H.-J.; Janshoff, A. Formation of Three-Dimensional Protein-Lipid Aggregates in Monolayer Films Induced by Surfactant Protein B. *Biophys. J.* **2000**, *79*, 904–918.
11. Malcharek, S.; Hinz, A.; Hilterhaus, L.; Galla, H.-J. Multilayer Structures in Lipid Monolayer Films Containing Surfactant Protein C: Effects of Cholesterol and POPE. *Biophys. J.* **2005**, *88*, 2638–2649.
12. Wang, L.; Cai, P.; Galla, H. J.; He, H.; Flach, C. R.; Mendelsohn, R. Monolayer-Multilayer Transitions in a Lung Surfactant Model: IR Reflection-Absorption Spectroscopy and Atomic Force Microscopy. *Eur. Biophys. J.* **2005**, *34*, 243–254.
13. Zhang, H.; Wang, Y. E.; Fan, Q.; Zuo, Y. Y. On the Low Surface Tension of Lung Surfactant. *Langmuir* **2011**, *27*, 8351–8358.
14. Bourdos, N.; Kollmer, F.; Benninghoven, A.; Ross, M.; Sieber, M.; Galla, H.-J. Analysis of Lung Surfactant Model Systems with Time-of-Flight Secondary Ion Mass Spectrometry. *Biophys. J.* **2000**, *79*, 357–369.
15. Nel, A.; Xia, T.; Madler, L.; Li, N. Toxic Potential of Materials at the Nanolevel. *Science* **2006**, *311*, 622–627.
16. Schleh, C.; Muhlfeld, C.; Pulskamp, K.; Schmiedl, A.; Nassimi, M.; Lauenstein, H.; Braun, A.; Krug, N.; Erpenbeck, V.; Hohlfeld, J. The Effect of Titanium Dioxide Nanoparticles on Pulmonary Surfactant Function and Ultrastructure. *Respir. Res.* **2009**, *10*, 90–100.
17. Bakshi, M. S.; Zhao, L.; Smith, R.; Possmayer, F.; Petersen, N. O. Metal Nanoparticle Pollutants Interfere with Pulmonary Surfactant Function *in Vitro*. *Biophys. J.* **2008**, *94*, 855–868.
18. Sung, J. C.; Pulliam, B. L.; Edwards, D. A. Nanoparticles for Drug Delivery to the Lungs. *Trends Biotechnol.* **2007**, *25*, 563–570.
19. Krol, S.; Janshoff, A.; Ross, M.; Galla, H.-J. Structure and Function of Surfactant Protein B and C in Lipid Monolayers: A Scanning Force Microscopy Study. *Phys. Chem. Chem. Phys.* **2000**, *2*, 4586–4593.
20. von Nahmen, A.; Post, A.; Galla, H.-J.; Sieber, M. The Phase Behavior of Lipid Monolayers Containing Pulmonary Surfactant Protein C Studied by Fluorescence Light Microscopy. *Eur. Biophys. J.* **1997**, *26*, 359–369.
21. von Nahmen, A.; Schenk, M.; Sieber, M.; Amrein, M. The Structure of a Model Pulmonary Surfactant As Revealed by Scanning Force Microscopy. *Biophys. J.* **1997**, *72*, 463–469.
22. Harishchandra, R. K.; Saleem, M.; Galla, H.-J. Nanoparticle Interaction with Model Lung Surfactant Monolayers. *J. R. Soc. Interface* **2010**, *7*, S15–S26.
23. Beake, B. D.; Leggett, G. J.; Shipway, P. H. Frictional, Adhesive and Mechanical Properties of Polyester Films Probed by Scanning Force Microscopy. *Surf. Interface Anal.* **1999**, *27*, 1084–1091.
24. DeVecchio, D.; Bhushan, B. Localized Surface Elasticity Measurements Using an Atomic Force Microscope. *Rev. Sci. Instrum.* **1997**, *68*, 4498–4505.
25. Radmacher, M.; Tillmann, R. W.; Gaub, H. E. Imaging Viscoelasticity by Force Modulation with the Atomic Force Microscope. *Biophys. J.* **1993**, *64*, 735–742.
26. Graf, C.; Schartl, W.; Maskos, M.; Schmidt, M. Tracer Diffusion of Polyorganosiloxane Nanoparticles in Solution: Effects of Tracer Topology and Particle Concentration. *J. Chem. Phys.* **2000**, *112*, 3031–3039.
27. Bar, G.; Rubin, S.; Parikh, A. N.; Swanson, B. I.; Zawodzinski, T. A.; Whangbo, M. H. Scanning Force Microscopy Study of Patterned Monolayers of Alkanethiols on Gold. Importance of Tip Sample Contact Area in Interpreting Force Modulation and Friction Force Microscopy Images. *Langmuir* **1997**, *13*, 373–377.
28. Reichelt, R.; Engel, A. Monte Carlo Calculations of Elastic and Inelastic Electron Scattering in Biological and Plastic Materials. *Ultramicroscopy* **1984**, *13*, 279–293.
29. Ross, M.; Steinem, C.; Galla, H.-J.; Janshoff, A. Visualization of Chemical and Physical Properties of Calcium-Induced Domains in DPPC/DPPS Langmuir–Blodgett Layers. *Langmuir* **2001**, *17*, 2437–2445.
30. Galla, H.-J.; Bourdos, N.; von Nahmen, A.; Amrein, M.; Sieber, M. The Role of Pulmonary Surfactant Protein C during the Breathing Cycle. *Thin Solid Films* **1998**, *327–329*, 632–635.
31. Choe, S.; Chang, R.; Jeon, J.; Violi, A. Molecular Dynamics Simulation Study of a Pulmonary Surfactant Film Interacting with a Carbonaceous Nanoparticle. *Biophys. J.* **2008**, *95*, 4102–4114.
32. Schneemilch, M.; Quirke, N. Molecular Dynamics of Nanoparticle Translocation at Lipid Interfaces. *Mol. Simul.* **2010**, *36*, 831–835.
33. Fan, Q.; Wang, Y. E.; Zhao, X.; Loo, J. S. C.; Zuo, Y. Y. Adverse Biophysical Effects of Hydroxyapatite Nanoparticles on Natural Pulmonary Surfactant. *ACS Nano* **2011**, *5*, 6410–6416.
34. Cleveland, J. P.; Anczykowski, B.; Schmid, A. E.; Elings, V. B. Energy Dissipation in Tapping-Mode Atomic Force Microscopy. *Appl. Phys. Lett.* **1998**, *72*, 2613–2615.
35. Garcia, R.; Magerle, R.; Perez, R. Nanoscale Compositional Mapping with Gentle Forces. *Nat. Mater.* **2007**, *6*, 405–411.
36. Zhao, Y.; Cheng, Q.; Qian, M.; Cantrell, J. H. Phase Image Contrast Mechanism in Intermittent Contact Atomic Force Microscopy. *J. Appl. Phys.* **2010**, *108*, 094311.
37. Boussu, K.; Van der Bruggen, B.; Volodin, A.; Snauwaert, J.; Van Haesendonck, C.; Vandecasteele, C. Roughness and Hydrophobicity Studies of Nanofiltration Membranes Using Different Modes of AFM. *J. Colloid Interface Sci.* **2005**, *286*, 632–638.
38. Kramer, A.; Liashkovich, I.; Ludwig, Y.; Shahin, V. Atomic Force Microscopy Visualises a Hydrophobic Meshwork in

the Central Channel of the Nuclear Pore. *Pfluegers Arch.* **2008**, *456*, 155–162.
39. Bar, G.; Thomann, Y.; Brandsch, R.; Cantow, H. J.; Whangbo, M. H. Factors Affecting the Height and Phase Images in Tapping Mode Atomic Force Microscopy. Study of Phase-Separated Polymer Blends of Poly(ethene-*co*-styrene) and Poly(2,6-dimethyl-1,4-phenylene oxide). *Langmuir* **1997**, *13*, 3807–3812.
40. Basnar, B.; Friedbacher, G.; Brunner, H.; Vallant, T.; Mayer, U.; Hoffmann, H. Analytical Evaluation of Tapping Mode Atomic Force Microscopy for Chemical Imaging of Surfaces. *Appl. Surf. Sci.* **2001**, *171*, 213–225.
41. James, P. J.; Antognozzi, M.; Tamayo, J.; McMaster, T. J.; Newton, J. M.; Miles, M. J. Interpretation of Contrast in Tapping Mode AFM and Shear Force Microscopy. A Study of Nafion. *Langmuir* **2001**, *17*, 349–360.
42. Rugonyi, S.; Biswas, S. C.; Hall, S. B. The Biophysical Function of Pulmonary Surfactant. *Respir. Physiol. Neurobiol.* **2008**, *163*, 244–255.
43. Oosterlaken-Dijksterhuis, M. A.; Haagsman, H. P.; van Golde, L. M.; Demel, R. A. Characterization of Lipid Insertion into Monomolecular Layers Mediated by Lung Surfactant Proteins SP-B and SP-C. *Biochemistry* **1991**, *30*, 10965–10971.
44. Ross, M.; Krol, S.; Janshoff, A.; Galla, H.-J. Kinetics of Phospholipid Insertion into Monolayers Containing the Lung Surfactant Proteins SP-B or SP-C. *Eur. Biophys. J.* **2002**, *31*, 52–61.
45. Klenz, U.; Saleem, M.; Meyer, M. C.; Galla, H.-J. Influence of Lipid Saturation Grade and Headgroup Charge: A Refined Lung Surfactant Adsorption Model. *Biophys. J.* **2008**, *95*, 699–709.
46. Utech, S.; Scherer, C.; Maskos, M. Multifunctional, Multicompartment Polyorganosiloxane Magnetic Nanoparticles for Biomedical Applications. *J. Magn. Magn. Mater.* **2009**, *321*, 1386–1388.
47. Haagsman, H. P.; Hawgood, S.; Sargeant, T.; Buckley, D.; White, R. T.; Drickamer, K.; Benson, B. J. The Major Lung Surfactant Protein, SP 28−36, Is a Calcium-Dependent, Carbohydrate-Binding Protein. *J. Biol. Chem.* **1987**, *262*, 13877–13880.
48. Baumann, F.; Deubzer, B.; Geck, M.; Dauth, J.; Sheiko, S.; Schmidt, M. Soluble Organosilicon Micronetworks with Spatially Confined Reaction Sites. *Adv. Mater.* **1997**, *9*, 955–958.